

A high density field reversed configuration (FRC) target for magnetized target fusion: First internal profile measurements of a high density FRC^{a)}

T. Intrator,^{1,b)} S. Y. Zhang,¹ J. H. Degnan,² I. Furno,¹ C. Grabowski,² S. C. Hsu,¹ E. L. Ruden,² P. G. Sanchez,¹ J. M. Taccetti,¹ M. Tuszewski,¹ W. J. Wagenaar,¹ and G. A. Wurden¹

¹Los Alamos National Laboratory, Los Alamos, New Mexico 87545

²Air Force Research Laboratory, Kirtland Air Force Base, Albuquerque, New Mexico 87117

(Received 31 October 2003; accepted 27 January 2004; published online 23 April 2004)

Magnetized target fusion (MTF) is a potentially low cost path to fusion, intermediate in plasma regime between magnetic and inertial fusion energy. It requires compression of a magnetized target plasma and consequent heating to fusion relevant conditions inside a converging flux conserver. To demonstrate the physics basis for MTF, a field reversed configuration (FRC) target plasma has been chosen that will ultimately be compressed within an imploding metal liner. The required FRC will need large density, and this regime is being explored by the FRX-L (FRC-Liner) experiment. All theta pinch formed FRCs have some shock heating during formation, but FRX-L depends further on large ohmic heating from magnetic flux annihilation to heat the high density ($2-5 \times 10^{22} \text{ m}^{-3}$), plasma to a temperature of $T_e + T_i \approx 500 \text{ eV}$. At the field null, anomalous resistivity is typically invoked to characterize the resistive like flux dissipation process. The first resistivity estimate for a high density collisional FRC is shown here. The flux dissipation process is both a key issue for MTF and an important underlying physics question. © 2004 American Institute of Physics. [DOI: 10.1063/1.1689666]

I. INTRODUCTION

Los Alamos National Laboratory leads an experimental effort to demonstrate the physics basis for a demonstration of magnetized target fusion (MTF). This paper explores the dissipation of magnetic energy in a field reversed configuration (FRC) via flux annihilation and the consequent ohmic heating; key to both the MTF applications and basic plasma physics questions. The first resistivity estimates for high density collisional FRCs are shown.

MTF is a subset of magneto-inertial fusion: pulsed, high-pressure approaches to fusion with inertial confinement of a plasma using magnetic field in an essential way. Examples include laser-heated solenoid plasmas, cryogenic fiber Z pinches, flow-stabilized Z pinches, and the composite $Z\theta$ pinch. MTF specifically requires an imploding pusher to compress and do work on the volume to heat a magnetized target plasma, such as a spheromak or FRC to fusion conditions. The MTF plasma regimes ($n \sim 10^{25} - 10^{26} \text{ m}^{-3}$ and $T \sim 5 \text{ keV}$) fall between magnetic fusion energy and inertial fusion energy.¹⁻³ Various flux conserving materials have been considered for the imploding pusher, including metal liners,⁴⁻⁶ gaseous or plasma pushers,⁷ and compressible liquid shells.^{8,9}

The FRX-L (FRC-Liner) experiment is our proposed physics demonstration of MTF, which could be a reduced-cost path to a more attractive fusion energy system. It requires a FRC¹⁰⁻¹² magnetized target plasma and its translation into a region where an imploding metal shell can

compress the plasma. Figure 1 shows a typical predicted trajectory for an FRC radius inside a cylindrical imploding shell. The constraints are a conserved adiabatic constant PV^γ , unity ratio of plasma particle pressure to external confining magnetic field $\beta \approx 1$, and 2.4 dimensional FRC compression. Field line tension causes axial contraction when the FRC is radially compressed,^{13,14} and the volume scales as $r^{2.4}$, i.e., more strongly than a two-dimensional compression proportional to r^2 .¹⁴

Compact toroids such as the spheromak and FRC have several potentially favorable features for this application:

- resilient, closed flux surfaces that maintain their topology during compression, as observed in compression and translation,^{13,15} stability experiments,¹⁶ and models;¹⁷
- lack of internal material objects facilitating compression within a liner; and
- ability to be translated from the plasma formation region into a liner for compression.

The FRC has been chosen as the candidate that can best survive formation, translation, and compression, starting at high density ($n \approx 10^{23} \text{ m}^{-3}$) before compression and increasing to $n > 10^{25} \text{ m}^{-3}$ after compression.^{18,19} As a plasma equilibrium it has high power density and $\beta = 1$. Other advantages of the FRC approach include:

- geometric simplicity, with no captured magnetic coils or center stack ohmic transformer;
- magnetic simplicity with no toroidal magnetic field or linked magnets;

^{a)}Paper CI23, Bull. Am. Phys. Soc. **48**, 50 (2003).

^{b)}Invited speaker.

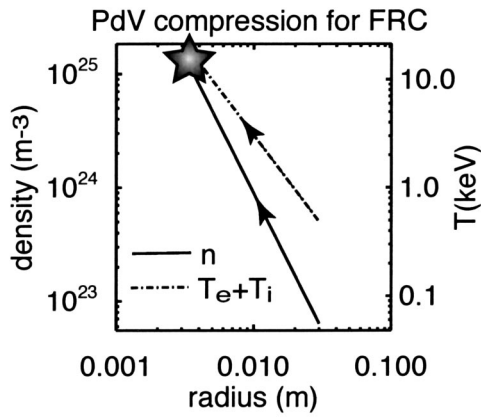


FIG. 1. Adiabatic PdV trajectory for an example FRC, $V \approx r^{2.4}$, $\beta \approx 1$, $PV^\gamma = \text{constant}$, initial density of approximately $5 \times 10^{22} \text{ m}^{-3}$, and initial temperature $T = T_e + T_i \approx 500 \text{ eV}$. Density (temperature) is shown with a solid (dashed) line.

- (c) heat exhaust handling via natural axial divertor;
- (d) advanced fuel potential could be realized at high β and large ion temperature; and
- (e) most initial physics research can transpire with existing facilities and technology.

A conceptual drawing is shown in Fig. 2, which calls out the plasma formation and injector region inside a conical theta pinch coil, and the radially imploding flux conserver region.

Formation of a FRC using high-voltage theta-pinch technology is well established, and the plasma characteristics of the FRC (i.e., stability, transport, and impurity content) in the density and temperature range of interest are reasonably well characterized. FRCs that are formed inductively have low impurity line radiation, i.e., $Z_{\text{eff}} \approx 1$. Open field lines outside the separatrix act as a natural divertor that isolates plasma loss flux from wall boundaries. These two attributes may substantially reduce impurity mixing, a concern for MTF. Early reversed-field theta pinches formed FRCs exceeding our target density^{20–22} but the diagnostic methods and theoretical understanding were less complete in the 1960s–70s.

The organization of this paper includes Sec. I, introduction; Sec. II, a discussion of the FRC physics linked with

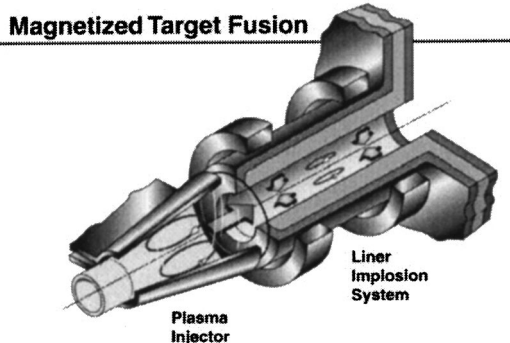


FIG. 2. MTF schematic, showing plasma formation region in a conical theta pinch coil on the left, and translation to a liner implosion section on upper right-hand corner.

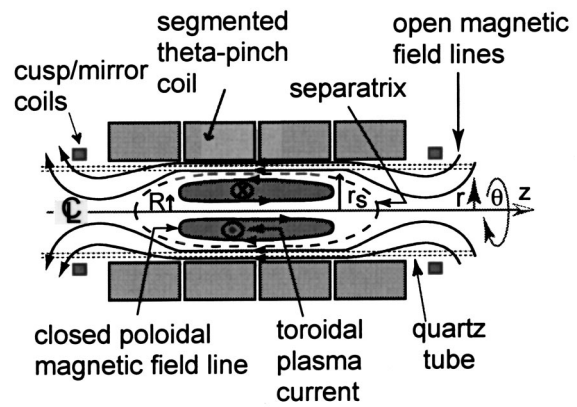


FIG. 3. FRC geometry and coordinate system including depictions of closed poloidal flux surfaces inside nearby open field lines, toroidal plasma current, and the flux conserving theta coil boundary.

resistivity investigations in Sec. III; a description in Sec. IV of the data analysis strategy; Sec. V, discussion of some implications; and a conclusion in Sec. VI.

II. FRC PHYSICS

This research focuses on demonstrating MTF with the FRC, but many scientific issues lie on this path. The FRC is extreme among magnetic configurations. There is high plasma $\beta \sim 1$, small (ideally zero) toroidal field, and the equilibrium is thought to be dominated by cross-field diamagnetic current and flows. These flows are likely to have large shear which is presently a topic of intense interest in plasma research. The FRC also has vanishing rotational transform, magnetic shear, and helicity which puts it in a class of equilibria that are apparently relaxed to a non force-free state. This is quite different from relaxation to zero β , which would be expected for a Taylor relaxation process. Stability lifetimes greatly exceed Alfvén times and defy MHD predictions. The underlying plasma physics that gives rise to these properties can be explored from the FRC standpoint. For example, strong flows may strongly influence plasma equilibria and stability. Generalized relaxation principles such as minimum dissipation theory^{23–25} may govern formation and equilibria. Many of these fundamental plasma physics questions extend beyond MHD single fluid models, and undoubtedly have analogs with geophysical and astrophysical phenomena.

The FRC is an elongated, self-organized compact toroid state that has toroidal plasma current and poloidal magnetic field. In Fig. 3 we indicate the closed-field-line torus inside a separatrix radius r_s separated from a flux conserving boundary by open-field-line sheath outside the separatrix. The equilibrium balances plasma pressure with radial magnetic field pressure and axial field-line “tension,” and it relates externally measurable to internal inferred quantities. The MHD presumption of radial pressure balance and instant equilibration along flux surfaces can be written $p_{\text{max}} = p(\Phi) + B_z(\Phi)^2/2\mu_0 = B_{\text{ext}}^2/2\mu_0$. We presume the internal variables are flux functions and define Φ as poloidal flux. For the ideal

straight cylinder, inclusion of axial pressure balance^{10,11} relates volume averaged pressure inside the separatrix $\langle p \rangle = \langle nT \rangle = \langle n(T_e + T_i) \rangle$ to the external magnetic field pressure $\langle \beta \rangle = 1 - x_s^2/2$. Here $x_s = r_s/r_c$, and r_c is the coil radius, $\langle \beta \rangle = \langle nT \rangle / (B_{\text{ext}}^2/2\mu_0)$, B_{ext} is the external separatrix magnetic field, n is the density, and T is the temperature. The radial size scale is several ion gyro radii $r_s/r_{Gi} \approx 2$, evaluated using the external (large) magnetic field B_{ext} . Because of this, temperatures across the FRC tend to be uniform.

III. FRC RESISTIVITY

The toroidal current decays in time as it ohmically heats the plasma particles. Resistive like diffusion relates poloidal flux annihilation time scale to the current density at the O point ($r=R$). Closed flux contours converge radially inward as flux annihilates. The total flux is global and measurements from the outside can be used to estimate the decay time scale for internal flux annihilation at the field null. We assume flux dissipation that can be described with an Ohm's law $E_\theta = \eta^* J_\theta + v \times B_z$ by invoking anomalous resistivity η^* . Presumably the flow vanishes at the O point $r=R$, so we ignore the Hall term. Poloidal flux is defined $\Phi_{\text{pol}} = \int_R^{r_s} B_z(r) 2\pi r dr$. Ampere's law relates the current density to derivatives of B_z , i.e., $\nabla \times B = \mu_0 J_\theta = \partial B_z(r)/\partial r$ which we will estimate later with internal experimental measurements of $\beta(r)$ gradients. The time dependence of $B_z(r,t)$ from Faraday's law is $\nabla \times E_\theta = -\partial B_z(r)/\partial t$ and can be integrated on a surface in the domain $R < r < r_s$. The flux annihilation rate at the O point is $E_\theta(R) = -\partial \Phi_{\text{pol}}/\partial t 2\pi R$, and using Ohm's law one can write the resistivity^{26,27} at the field null as

$$\eta(R)/\mu_0 = -(\partial \Phi/\partial t)/[2\pi R \partial B_z(r)/\partial r]. \quad (1)$$

Assuming continuity of particle loss flux at the edge, one can also use similar arguments to evaluate resistivity at the separatrix²⁸

$$\eta_{\text{eff}}(r_s)/\mu_0 = -r_s \langle n \rangle (1 - \beta_s) / [\tau_N n_s \partial \beta(r=r_s)/\partial r], \quad (2)$$

where τ_N is the experimental particle inventory decay time ($\tau_N \approx 10 \mu\text{s}$ in FRX-L).

High density FRCs in FRX-L are formed using a theta pinch fast magnetic pulse. The desired total temperature is $T = T_e + T_i \approx 500 \text{ eV}$, so heating mechanisms are at once a practical concern for MTF applications and a basic physics issue. During formation there is initially some shock heating but we rely on subsequent ohmic heating from magnetic flux annihilation to heat the plasma. The typical FRC anomalous resistivity η^* is much larger than Spitzer Coulomb resistivity η_s . On the other hand, FRX-L can operate in a regime that should be dominated by Coulomb collisionality. Figure 4 surveys several FRC experiments, where we plot the scale size of each FRC (excluded flux radius r_s) normalized to the coulomb electron-ion scattering mean free path (λ_{ei}). The horizontal axis displays density normalized to a reference line density N^* (particles per unit length), which is the density of a $\beta=1$ cylindrical column with radius of one ion skin depth (referenced to peak density) or equivalently one ion gyro radius (referenced to maximum B_{ext}). High density

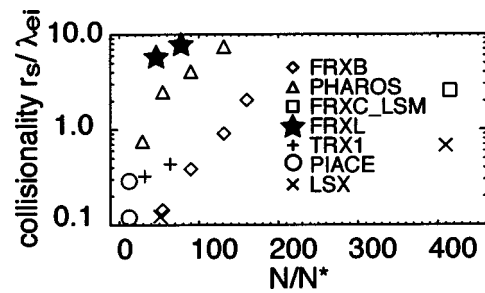


FIG. 4. Survey of FRC experiments showing a range of Coulomb collisionality regimes. The electron-ion collision mean free path is plotted against dimensionless line density. A convenient formula is $N/N^* = 3.2p_0$ (mTorr) r_{wall} (m), where p_0 is the neutral fill pressure, and the wall radius is given by r_{wall} . We reference information about experiments PHAROS (see Ref. 20), TRX-1 (see Ref. 27), PIACE (see Ref. 29), LSX (see Ref. 30), TRX-2 (see Ref. 31), FRX-B (see Ref. 10), and FRXC-LSM (see Ref. 28).

FRC experiments such as PHAROS²⁰ with less complete profile diagnostics than FRX-L have been studied.^{21,22} There is some resistivity data extant for Triggered Reconnection Experiment (TRX-1),²⁷ Plasma Injection and Adiabatic Compression Experiment (PIACE),²⁹ Large S Experiment (LSX),³⁰ TRX-2,³¹ and Field Reversed Configuration Experiment C-Large Source Modification (FRXC-LSM),²⁸ which are substantially less collisional. One might naively assume that Spitzer resistivity dominates the ohmic heating physics. In the following the first resistivity estimates for high density collisional FRCs are shown.

IV. DATA ANALYSIS

The theta pinch approach is used to trap some fraction of the initial bias field. The internal flux is estimated¹⁰ from the relation $\Phi_{\text{int}} \approx \pi r_c^2 B_{\text{ext}} (x_s/2^{1/2})^{3+\epsilon}$ to be approximately 0.4 m Wb at formation and decays smoothly during equilibrium. Here B_{ext} is the measured axial magnetic field used for the excluded flux data, ϵ is a profile dependent parameter that falls between 0 (high flux sharp boundary limit) and 1 (low flux sharp boundary limit). The choice of $\epsilon \approx 0.25$ is consistent with past FRC experiments at LANL.¹⁰ Estimates of the flux confinement time τ_ϕ are derived from the e -folding loss time from Fig. 5, which displays typical shot parameters.

The separatrix radius r_s can be inferred from axial magnetic flux loop data³² and a local magnetic field value B_{ext} in the region outside the separatrix and inside the theta coil wall radius r_c . The ellipsoidal FRC volume can be approximated from excluded flux radius data at several axial locations. Particle confinement time $\tau_N \approx 10 \mu\text{s}$ follows from the particle inventory, which is a volume integral of the density measurements. Using the average $\langle \beta \rangle$ condition and pressure balance yields for Fig. 5 an average temperature $\langle T_e + T_i \rangle \approx 180 \text{ eV}$ during the equilibrium period ($10.5 \mu\text{s} < t < 18 \mu\text{s}$). The excluded flux array together with the multichord interferometer provide essential information on FRC formation and equilibrium.

The eight chord interferometer was located at the axial midplane. These data were inverted to estimate density profiles, and Abel inverted contours for shot 2027 are displayed with radius as the horizontal axis and time on the vertical

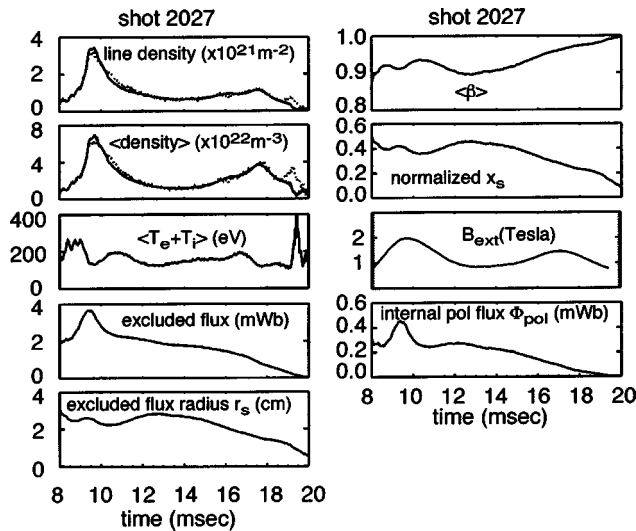


FIG. 5. Diagnostic traces for the shot used in the resistivity analysis. Line density, excluded flux, and external magnetic field B_{ext} are measured. Volume averaged $\langle \beta \rangle$ is used to infer the other characteristics.

axis in Fig. 6 in units of 10^{22} m^{-3} . Overlaid are the calculated excluded flux radius r_s (dash-dot line), and field null radius at $R = r_s / (2)^{1/2}$ (dashed line). Two horizontal dotted lines indicate radial cuts across this data set at times $t = 11.22$ and $11.82 \mu\text{s}$. Figure 7 shows two radial density profiles on the top plot and assuming flat temperature profiles and $T_e \approx T_i$, two profiles of the inferred $\beta(r)$ on the bottom plot. The interferometer chord locations are indicated on the figure by the boxes. Representative error bars for the density profiles were estimated from the dispersion of data before smoothing in the time domain. It is clear that these profiles are hollow, with the density at $r=0$ approximately 50% of the density maximum near $r=R$. The solid line on each plot indicates an example rigid rotor profile prediction for $n(r)$ and $\beta(r)$. The radial gradients for $r < R$ are somewhat less than the rigid rotor predictions. In the near future more interferometer chords will be clustered in the large gradient central $r < R$ and $r \approx r_s$ edge regions of the FRC. The rigid

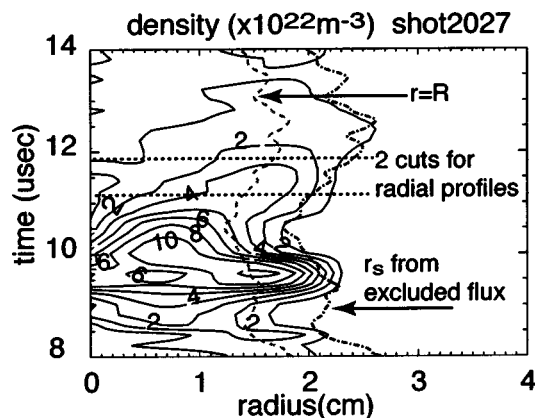


FIG. 6. Contours of density plotted in a time-radius plane, extracted from multichord interferometer data. The magnetic separatrix (field null) radius as a function of time is indicated by the dash-dot (dash) line. Radial cuts from Fig. 7 are taken at times shown by the horizontal dotted lines.

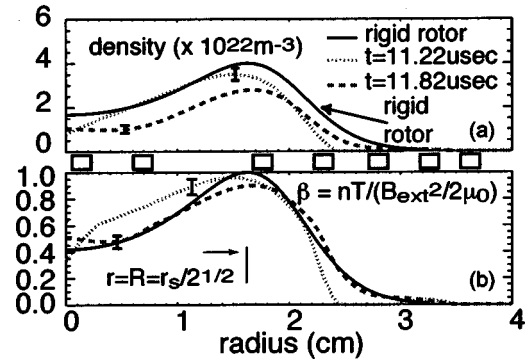


FIG. 7. Comparison of radial cuts of (a) density $n(r)$ and (b) inferred $\beta(r)$ profile data at two times (dotted and dashed) with sample rigid rotor model profiles (solid line). The fit parameters are $\tau_\phi = 5.0 \mu\text{s}$, $\langle \beta \rangle = 0.8$, $T = T_e + T_i = 200 \text{ eV}$, $r_s = 2.3 \times 10^{-2} \text{ m}$, shape $k = 1.0$. Interferometer chord locations are indicated by the squares between (a) and (b), and the estimated error bars are displayed on the plots.

rotor model equations for $J_\theta \times B_z = \nabla p$ assume flat $T(r)$ so that the magnetic field profile is $B_z(r)/B_{ext} = \tanh[k(r^2/R^2 - 1)]$, and the plasma pressure is $\beta(r) = \{\cosh[k(r^2/R^2 - 1)]\}^{-2} \alpha n$. The resistivity at the field null can be evaluated using the rigid rotor model profiles with the inclusion of an experimentally measured flux loss time τ_ϕ :

$$\eta(R)/\mu_0 = [R^2/4\tau_\phi][\ln \cosh(k)]/k^2. \quad (3)$$

The resistivities at the field null $r=R$ and at the separatrix $r=r_s$ are shown in Fig. 8, assuming a clean plasma $Z_{eff} = 1$. An optical multichannel analyzer with scanning gate shorter than $10 \mu\text{s}$ was used to verify that these shots had small impurity line radiation. The top plot shows the time history of the poloidal flux with two exponential fits. The error bars

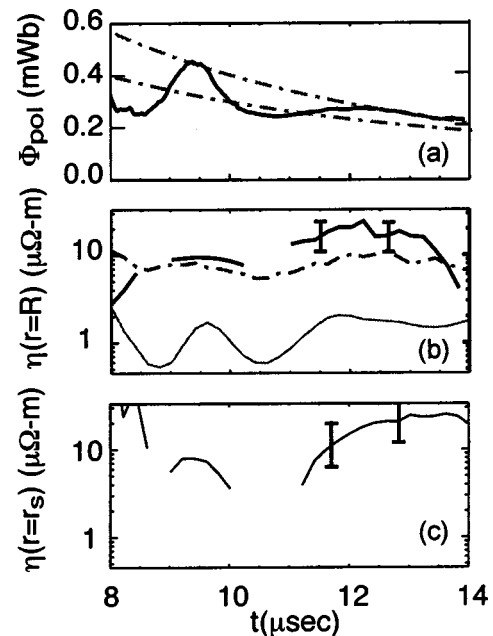


FIG. 8. Top panel (a) shows time history of poloidal flux with two exponentially decaying fits that form part of the error bar analysis; middle panel (b) shows Spitzer (solid), rigid rotor (dash-dots), and FRX-L profile (solid with error bars) resistivities; and bottom panel (c) shows estimated edge resistivity. The estimated error bars are displayed on the plots.

are estimated from the uncertainties in the flux confinement time and the Abel inverted $n(r)$ [and, hence, $\beta(r)$]. We used a range of time constants with upper and lower limits of $\tau_{\Phi} = 6$ and $8 \mu\text{s}$ indicated as the dashed lines on the plot. The time variations in the data from Fig. 7 indicate some dynamic contours, so that the net error bars are larger than the uncertainty in the τ_{Φ} from Fig. 8. Figure 8(b) shows the Spitzer resistivity $\eta_S \approx 1\text{--}2 \mu\Omega \text{ m}$, estimated from the electron temperature taken to be $T_e \approx (T_c + T_i)/2$ from Fig. 5. The rigid rotor resistivity is indicated by the dash-dot line, and the calculated experimental resistivity $\eta^* \approx 10\text{--}25 \mu\Omega \text{ m}$, is shown by the top solid line with error bars overlaid. The bottom panel Fig. 8(c) tracks the estimated resistivity $\eta_{\text{sep}}^* \approx 10\text{--}25 \mu\Omega \text{ m}$ at the separatrix. This is not too different from the values at the field null. The dropouts in the plot correspond to where the calculated excluded flux radius fails to track the interferometer density edge sufficiently well, and the estimated edge gradient gets vanishingly (and unrealistically) small. The resistivities appear to exceed the rigid rotor estimates and are 10–20 times the Spitzer resistivity.

V. DISCUSSION

Flux retention is a key issue for the FRC as target plasma for MTF. The underlying physics sets the internal resistivity, flux burnup, heating rates, and the equilibrium profiles. Since the separatrix radius is so much larger than the electron-ion collision mean free path, FRX–L is highly collisional in this respect. Therefore, one might expect the resistivity to be dominated by Spitzer resistivity. The measured resistivity seems to be anomalously larger than this by a factor of 10–20 at least. The electron temperature would need to be much lower than our estimate (e.g., 10%–20% of $T_e \approx T/2$) to account for this discrepancy. The microphysics driving this anomalous resistivity is still not known. It may be that a collisionless MHD plasma is not required to study some of the causes of anomalous resistivity, or even that examples of magnetic reconnection and dynamo could occur in a collisional plasma. Better temperature data would be required to address transport associated with ion viscosity, which invokes a collisionality parameter r_s/λ_{ii} . If electron and ion temperatures are equal then $\lambda_{ii} = \lambda_{ei}$, but without this presumption r_s/λ_{ei} differs from r_s/λ_{ii} normalized to ion–ion mean free path (λ_{ii}).

The rigid rotor results shown in Fig. 7 invoke the model radial profiles and the experimentally measured flux loss time. The resistivity calculated from the data use the actual measured density and beta profiles. Thus if there is any difference in estimated resistivity it would be due to the difference in radial profiles. A larger resistivity would correspond to a gentler gradient in beta, because the increased anomalous flux diffusion rate η^*/μ_0 tends to flatten out the profiles. Given the error bars, we cannot cleanly distinguish between the model and data gradients. The rigid rotor model presumes zero shear in the plasma flow, and radially constant resistivity. This assumption may be valid except near the separatrix.

There is probably hidden density dependence in the η^* behavior. It is also likely that large changes in the internal

physics may have much smaller effects on the $\beta(r)$ profile. For instance if the heat flux through a volume was large, the product of $n(r)T(r)$ might vary little, while each one changed radically. Better internal profile measurements would therefore be very useful to investigate the physics inside the FRC. For instance flow measurements utilizing vacuum ultraviolet spectroscopy would avoid micro field broadening due to the large density and allow Doppler shift measurements of internal flows. Faraday rotation techniques are being developed to measure the magnetic field profiles inside the separatrix.

VI. SUMMARY

The FRX–L experiment is on-line, and being used to explore a wide range of operating parameters. Flux confinement and annihilation is both a practical and a physics issue, because the experiment relies upon flux annihilation to heat the plasma. These processes are characterized here by the anomalous resistivity η^* . FRX–L operates at the extremum of collisionality compared with other FRC experiments. Data show that FRX–L profiles are not far from rigid rotor predictions. The resistivity η^* is of the same order or somewhat larger than rigid rotor predictions, but anomalously larger (10–20 \times) than classical Coulomb resistivity η_S .

ACKNOWLEDGMENT

This work was supported by the United States Department of Energy, Office of Science and Technology Contract No. W-7405-ENG-36.

- ¹R. C. Kirkpatrick, I. R. Lindemuth, and M. S. Ward, *Fusion Technol.* **27**, 201 (1995).
- ²R. E. Siemon, I. R. Lindemuth, and K. F. Schoenberg, *Comments Plasma Phys. Controlled Fusion* **18**, 363 (1999).
- ³D. D. Ryutov and R. E. Siemon, *Comments Plasma Phys. Controlled Fusion* **2**, 185 (2001).
- ⁴T. Intrator, J. M. Taccetti, D. A. Clark, J. H. Degnan, D. Gale, S. K. Coffey, J. Garcia, P. Rodriguez, W. Sommars, B. Marshall, F. Wysocki, R. Siemon, R. Faehl, K. Forman, R. Bartlett, T. Cavazos, M. H. Frese, D. Fulton, J. C. Gueits, T. W. Hussey, R. Kirkpatrick, G. F. Kiuttu, F. M. Lehr, J. D. Letterio, I. Lindemuth, W. McCullough, R. Moses, R. E. Peterkin, R. E. Reinovsky, N. F. Roderick, E. L. Ruden, K. F. Schoenberg, D. Scudder, J. Shlachter, and G. A. Wurden, *Nucl. Fusion* **42**, 211 (2002).
- ⁵J. M. Taccetti, T. P. Intrator, F. J. Wysocki, K. C. Forman, D. G. Gale, S. K. Coffey, and J. H. Degnan, *Fusion Sci. Technol.* **41**, 13 (2002).
- ⁶J. H. Degnan, J. M. Taccetti, T. Cavazos, D. Clark, S. K. Coffey, R. J. Faehl, M. H. Frese, D. Fulton, J. C. Gueits, D. Gale, T. W. Hussey, T. P. Intrator, R. C. Kirkpatrick, G. H. Kiuttu, F. M. Lehr, J. D. Letterio, I. Lindemuth, W. F. McCullough, R. Moses, R. E. Peterkin, R. E. Reinovsky, N. F. Roderick, E. L. Ruden, J. S. Shlachter, K. F. Schoenberg, R. E. Siemon, W. Sommars, P. J. Turchi, G. A. Wurden, and F. J. Wysocki, *IEEE Trans. Plasma Sci.* **29**, 93 (2001).
- ⁷Y. C. F. Thio, E. Panarella, R. C. Kirkpatrick, C. E. Knapp, F. J. Wysocki, and G. R. Schmidt, in *Current Trends in International Fusion Research: Proceedings of the Second Symposium*, edited by E. Panarella (National Research Council Canada, Ottawa, Canada, 1999).
- ⁸P. J. Turchi, A. L. Cooper, R. Ford, and D. J. Jenkins, *Phys. Rev. Lett.* **36**, 1546 (1976).
- ⁹P. J. Turchi, A. L. Cooper, R. D. Ford, D. J. Jenkins, and R. L. Burton, in *Megagauss Technology and Pulsed Power Applications*, edited by P. J. Turchi (Plenum, New York, 1980), p. 375.
- ¹⁰M. Tuszewski, *Nucl. Fusion* **28**, 2033 (1988).

- ¹¹A. L. Hoffman, R. D. Milroy, J. T. Slough, and L. C. Steinhauer, *Fusion Technol.* **9**, 48 (1986).
- ¹²W. T. Armstrong, R. K. Linford, J. Lipson, D. A. Platts, and E. G. Sherwood, *Phys. Fluids* **24**, 2068 (1981).
- ¹³D. J. Rej, W. T. Armstrong, R. E. Chrien, P. L. Klingner, R. K. Linford, K. F. McKenna, E. G. Sherwood, R. E. Siemon, M. Tuszewski, and R. D. Milroy, *Phys. Fluids* **29**, 852 (1986).
- ¹⁴R. L. Spencer, M. Tuszewski, and R. K. Linford, *Phys. Fluids* **26**, 1564 (1983).
- ¹⁵H. Kever, *Nucl. Fusion Suppl.* **2**, 613 (1962).
- ¹⁶M. Tuszewski, D. P. Taggart, R. E. Chrien, D. J. Rej, R. E. Siemon, and B. L. Wright, *Phys. Fluids B* **3**, 2856 (1991).
- ¹⁷R. D. Milroy and J. U. Brackbill, *Phys. Fluids* **25**, 775 (1982).
- ¹⁸G. A. Wurden, K. F. Schoenberg, R. E. Siemon *et al.*, *J. Plasma Fusion Res.* **2**, 238 (1999).
- ¹⁹J. M. Taccetti, T. P. Intrator, G. A. Wurden, S. Y. Zhang, R. Aragonéz, P. N. Assmus, C. M. Bass, C. Carey, S. A. deVries, W. J. Fienup, I. Furno, S. C. Hsu, M. P. Kozar, M. C. Langner, J. Liang, R. J. Maqueda, R. A. Martinez, P. G. Sanchez, K. F. Schoenberg, K. J. Scott, R. E. Siemon, E. M. Tejero, E. H. Trask, M. Tuszewski, W. J. Waganaar, C. Grabowski, E. L. Ruden, J. H. Degnan, T. Cavazos, D. G. Gale, and W. Sommers, *Rev. Sci. Instrum.* **74**, 4314 (2003).
- ²⁰A. C. Kolb, W. H. Lupton, R. C. Elton, E. A. McLean, M. Swartz, M. P. Young, H. R. Griem, and E. Hintz, *Plasma Phys. Controlled Nucl. Fusion Res.* **1**, 261 (1965).
- ²¹A. Kaleck, L. Könen, P. Noll, K. Sugita, F. Waelbroeck, K. Watanabe, and H. Witulski, *Plasma Physics and Controlled Nuclear Fusion Research (Proceedings of the Third International Conference, Novosibirsk, 1968)* (International Atomic Energy Agency, Vienna, 1969), p. 581.
- ²²A. Eberhagen and W. Grossmann, *Z. Phys.* **248**, 130 (1971).
- ²³D. Montgomery and L. Phillips, *Phys. Rev. A* **38**, 2953 (1988).
- ²⁴R. Bhattacharyya, M. S. Janaki, and B. Dasgupta, *Phys. Lett. A* **291**, 291 (2001).
- ²⁵L. C. Steinhauer and A. Ishida, *Phys. Rev. Lett.* **79**, 3423 (1997).
- ²⁶M. Tuszewski and R. Linford, *Phys. Fluids* **25**, 765 (1982).
- ²⁷A. L. Hoffman, R. D. Milroy, and L. C. Stienhauer, *Appl. Phys. Lett.* **41**, 31 (1982).
- ²⁸R. E. Chrien and S. Okada, *Phys. Fluids* **30**, 3574 (1987).
- ²⁹S. Okada, Y. Kiso, S. Goto, and T. Ishimura, *Phys. Fluids B* **1**, 2422 (1989).
- ³⁰A. L. Hoffman, L. N. Carey, E. A. Crawford, D. G. Harding, T. E. DeHart, K. F. McDonald, J. L. McNeil, R. D. Milroy, J. T. Slough, R. Maqueda, and G. A. Wurden, *Fusion Technol.* **23**, 185 (1993).
- ³¹R. D. Milroy and J. T. Slough, *Phys. Fluids* **30**, 3566 (1987).
- ³²M. Tuszewski, *Phys. Fluids* **24**, 2126 (1981).